Lab on a Chip

Accepted Manuscript

ROYAL SOCIETY OF CHEMISTRY

www.rsc.org/loc

Graphical Abstract

The focused plug is in motion and dispersed in depletion zone while the enrichment zone shows a stationary focused plug.

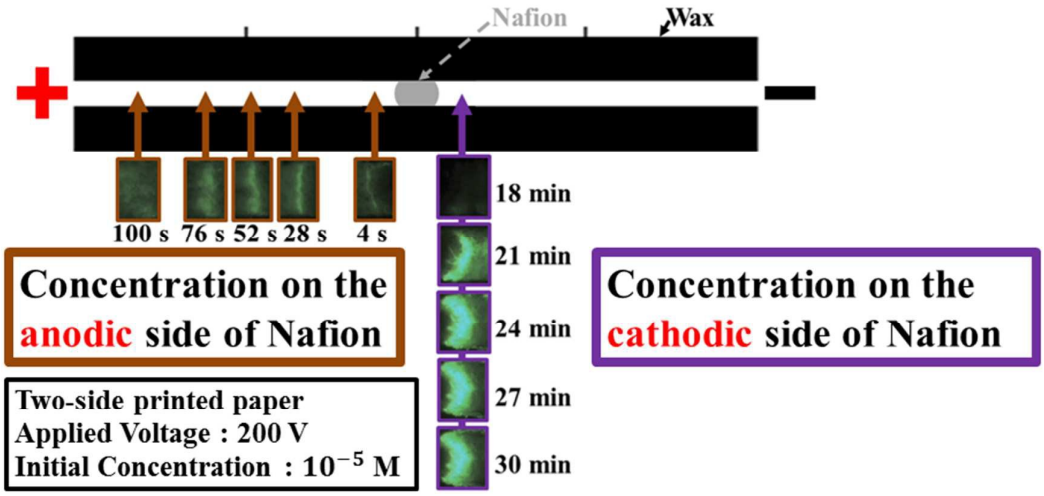

A proposed paper submitted to the

Lab on a Chip

Sample pre-concentration with high enrichment factors at a fixed location in paper-based microfluidic devices

By

Shih-Hao Yeh [1] and Ruey-Jen Yang[1]

[1] Department of Engineering Science, National Cheng Kung University, Tainan, Taiwan

Corresponding author: Prof. Ruey-Jen Yang

Tel：+886-6-2757575 extn 63343

Fax : +886-6-2766549

Email : rjyang@mail.ncku.edu.tw

Abstract

Lack of sensitivity is a major problem among microfluidic paper-based analytical devices (μPADs) for early disease detection and diagnosis. Accordingly, the present study presents a method for improving the enrichment factor of low-concentration biomarkers by using shallow paper-based channels realized using a double-sided wax-printing process. In addition, the enrichment factor is further enhanced by exploiting the ion concentration polarization (ICP) effect on the cathodic side of the nanoporous membrane, in which a stationary sample plug is obtained. The occurrence of ICP on the shallow-channel μPAD is confirmed by measuring the current-voltage response as the external voltage is increased from 0 to 210 V (or the field strength is from 0 to 1.05×10^4 V/m) over 600 s. In addition, to the best of our knowledge, the electroosmotic flow (EOF) speed on the μPAD fabricated by wax-channel is measured for the first time using a current monitoring method. The experimental results show that for a fluorescein sample, the concentration factor is increased from 130-fold in a conventional full-thickness paper channel to 944-fold in the proposed shallow channel. Furthermore, for a fluorescein isothiocyanate labeled bovine serum albumin (FITC-BSA) sample, the proposed shallow-channel μPAD achieves a 835-fold improvement in the concentration factor. The concentrating technique presented here provides a novel strategy for enhancing the detection sensitivity of μPADs applications.

1. Introduction

Microfluidic paper-based analytical devices (μPADs) are inexpensive, easy-to-use, disposable, and versatile diagnostic platforms. As such, they are ideally suited to point-of-care (POC) applications; particularly in developing regions of the world with less advanced medical infrastructures. Various methods are available for the fabrication of μPADs, including wax printing[1] where wax is printed on paper by a wax printer and then heated by a hotplate to form channels; photolithography[2-4] where exposed photoresist is used to define hydrophilic channels; plasma oxidation[5] where hydrophilic channels are fabricated on hydrophobized paper by plasma treatment; plotting[6] where hydrophobic PDMS is printed by a plotter to define hydrophilic channels; inkjet printing[7] where toluene printed by an inkjet printer makes hydrophobized paper hydrophilic; and cutting[8, 9] where channels are shaped by a computer-controlled blade. In μPAD-based assays, sensing is performed using fluorescence,[10-13] chemiluminescence,[14-17] electrochemiluminescence,[18, 19] electrochemical,[20, 21], or colorimetric[22, 23] techniques. However, the sensitivity of such assays is generally insufficient to detect biomarkers with low concentrations in body fluids, and hence numerous false negatives occur. The present study thus considers the problem of increasing the assay sensitivity by means of an enhanced ion concentration polarization (ICP) effect.

The literature contains many methods for enhancing the concentration of samples in liquids, including ICP,[24-28] isotachophoresis (ITP),[29, 30, 42], field-amplified sample stacking (FASS),[31] and micellar electrokinetic sweeping.[32] Rosenfeld and Bercovici[42] presented a novel μPAD utilizing ITP and demonstrating 1000-fold gain in peak concentration. Many researchers have shown that ICP can be induced at a micro-nano interface given the application of a voltage in the limiting current region.[33, 34] Moreover, several researchers have demonstrated the use of ICP in performing sample pre-concentration on μPADs.[35-38] Gong et al[35] applied paper-device to concentrate protein, FITC-BSA, extending its limits of detection from ~10 to ~2 pmol/mL, i.e., 5-fold concentration gain factor. Yang et al[36] demonstrated 15-fold improvement in the sample concentration of

FITC-BSA by using their proposed optimal convergent-channel μPAD design. Phan et al[37] demonstrated 60-fold concentration enhancement of fluorescent dye samples achieved within 200 sec. They focused target species in the depletion zone with plastics to cover the μPAD channel. The use of the plastic cover may hinder heat dissipation. In addition they need to create a field for balancing electrophoresis and electroosmotic flow. Gong et al[38] showed direct Hepatitis B virus DNA analysis with paper-based ICP, and demonstrates 100-fold increase in the signal of the pre-core fragment achieved following pre-concentration and separation. However, the concentration factor of these μPADs devices is still generally much lower than that of non-paper-based microfluidic devices. As a result, more effective ICP-based sample concentration schemes on μPADs are required.

Accordingly, the present study proposes a method for enhancing the ICP preconcentration effect by reducing the μPAD channel depth using a two-sided wax-printing process. In addition, a method is presented for concentrating the sample and fixing it at the location near the cathodic side of Nafion by means of an ICP effect. The feasibility of the proposed device is demonstrated by comparing the sample concentration achieved for a pure fluorescein sample in the proposed shallow-channel μPAD with that obtained in a full-thickness μPAD prepared using a traditional single-sided wax-printing technique. The feasibility of the proposed shallow-channel design for practical protein applications is then demonstrated by performing the preconcentration of a fluorescein isothiocyanate labeled bovine serum albumin (FITC-BSA) sample. The method presented here is beneficial to researchers attempting to enhance the detection sensitivity of μPADs.

2. Materials and Methods

2.1 Materials and Device Fabrication

Wax printing has many advantages for the fabrication of μPADs,[1, 39, 40] including a low cost, good versatility, a straightforward process, and the potential for mass production. In addition, wax is

compatible with aqueous solutions, and hence less chemical reaction occurs during experiment. In a typical wax-printing process, hydrophobic wax barriers are designed using commercial software (e.g., AutoCAD) and the wax is then penetrated into the paper substrate by capillary forces under the effects of heating. The present study fabricates two wax-printed μPADs, namely a conventional μPAD in which the substrate is printed with wax on one side of the paper only, and the wax then penetrates through the full thickness of the paper under heating, and a second device in which the substrate is printed with wax on both sides of the paper, and the wax layers penetrate the paper under a careful thermal control by a laminator. The former device thus contains a hydrophilic channel which extends through the entire thickness of the paper, while the latter device contains a shallow channel only (see Fig. 1). It is expected that the shallow channel (~50 μm) has four main advantages for ICP-induced sample concentration, namely (1) a lower electroosmotic flow (EOF) velocity due to a less zeta potential of the wax than that the of fiber;[41] (2) the ability to apply a higher voltage across the device due to the rapid heat dissipation;[42] (3) a greater confinement of the concentrated sample due to its smaller space;[36] and (4) a greater signal visibility due to smaller channel thickness, i.e.,[43]

$$Signal\ visibility\ (\%) = \frac{Visible\ depth\ (\sim 10 \mu m)}{Membrane\ thickness} \quad (1)$$

The μPADs were fabricated from cellulose filter paper (Whatman qualitative filter paper, Grade 1). The paper was deliberately chosen due to its high porosity, i.e., 0.76 ± 0.01, as evaluated using Eq. (2) below[44]:

$$\varepsilon_p = \frac{w_{wet} - w_{dry}}{\beta_{total} \times \rho_{water}} \quad (2)$$

where ε_p is the porosity; w_{dry} and w_{wet} are the weights of the paper when dry and when filled with water, respectively; β_{total} is the total volume of the paper, and ρ_{water} is the density of water. The cellulose paper with higher porosity contains less fiber and allows better see-through condition, and hence the sample signal can be better detected. In addition to its high porosity, the cellulose

paper also has only weak interaction with biomolecules[45] and does not require the use of external forces, such as a pump, to induce capillary fluid transport.[46, 47]

Figure 1 shows the main steps in the fabrication process for a conventional μPAD (left) and the shallow-channel μPAD proposed in this study (right). In both cases, the hydrophobic wax barriers were printed using a commercial wax printer (Xerox ColorQube 8570). For the conventional device, wax was printed on one side of the paper only, and the substrate was then placed in a high temperature oven (VULCAN A-550) at a temperature of 155 ℃ for 90 s to allow the wax to penetrate through the full thickness of the paper. For the μPAD printed on both sides of the paper, the substrate was inserted into a temperature-controlled laminator (HK330DS) such that the wax coatings on either side of the substrate wicked into the paper. Notably, the laminator provides a uniform and controllable heating effect, and therefore allows the depth of the hydrophilic channel to be accurately controlled. In the present study, a shallow channel with a depth of approximately 50 μm was realized by setting the lamination temperature to 125 ℃ and the feeding speed as 20 mm/s. (Note that the average depth of the channel was determined by cutting the μPAD along the perpendicular direction of the channel, placing the paper between two glass slides, and then observing the cross-sectional view through a microscope (Fig. 1(d)).

As shown in Fig. 1(c), the channel in the one-side printed device had dimensions of 20 mm x 1.3 mm x 180 μm (length x width x thickness). The channel in the two-side printed device had an identical length and width. However, as commented above, the channel depth was approximately equal to 50 μm. For both devices, the channel had a simple straight-line configuration Moreover, in both devices, a permselective membrane was fabricated by dripping 0.3 μL of Nafion (DuPont Fluoroproducts, DE-2020) on the central region of the channel and then allowing the solution to dry under ambient temperature conditions. Nafion was deliberately chosen as the membrane material since the fabrication process is simple[50-52] and its surface conductivity is high.[53]

To keep the paper channel horizontal and open to the atmosphere, the μPADs were simply clamped in place between four magnets. The reservoirs were realized using PDMS plates bonded to a glass slide, thereby allowing for the easy control of the reservoir location and dimensions (see Fig. 2). Finally, copper wires with a diameter of 1 mm were used as electrodes and placed in the reservoirs, each of which contained 30 μL of analyte solution. In evaluating the ICP performance of the proposed double-side printed μPAD, 10^{-2} M Tris (Tris (hydroxymethyl) Aminomethane EQP-ACS) buffer was used as the background electrolyte. Furthermore, the EOF velocity was measured using Tris buffers with concentrations of 10^{-2} M and 0.95×10^{-2} M, respectively.[48] The concentration effect in the proposed shallow-channel μPAD was evaluated using a fluorescein sample (fluorescein disodium salt dehydrate, 98+%, Alfa Aesar, USA) diluted to a final concentration of 10^{-8} M by mixing with 10^{-2} M Tris. Finally, the practical feasibility of the proposed double-side printed μPAD was evaluated using a fluorescein isothiocyanate labeled bovine serum albumin (FITC-BSA, Sigma-Aldrich, USA) sample; also diluted with 10^{-2} M Tris buffer to a final concentration of 10^{-8} M.

Yang et al[36] demonstrated that a convergent-channel can enhance concentration gain. Here the straight channel geometry due to its geometric symmetry on both sides of the coated Nafion membrane is adopted. The purpose is to compare the difference between the depletion effect on the cathodic side and the enrichment effect on the anodic side along the channel.

2.2 Experimental setup

The sample concentration effect within the two μPADs was observed using a mercury-lamp-induced fluorescence technique. The fluorescence signal was observed through an inverted fluorescence microscope (Nikon Eclipse Ti-E, Japan) interfaced with a CCD camera (DBK 41BU02, Imaging Source, Germany) fitted with IC Capture (V.2) software. The fluorescence intensity of the captured images was analyzed quantitatively using Image J software and Excel. The

external electrical field required to induce the ICP phenomenon was provided by a commercial power supply (EC1000S, NF Corporation, Japan). Finally, the current-voltage response of the μPADs was measured using a sourcemeter (Model 2400, Keithley Instruments, USA) equipped with LabTracer 2.0 software.

3. Results and Discussion

To confirm the ability of the two μPADs to induce the ICP phenomenon, the current-voltage response of each device was measured using a 10^{-8} M fluorescein solution in 10^{-2} M Tris buffer as the voltage was increased from 0 to 210 V (or the field strength was from 0 to 1.05×10^4 V/m) in 105 discrete steps over a period of 600 s. The corresponding results are shown in Fig. 3. It is seen that both I-V curves comprise three distinct regions. In region A (the under-limiting region), the current increases linearly with the voltage. In other words, the conductance of the system remains constant. In region B (the limiting-current region), the current (defined as the limiting current) increases only very slowly with the voltage due to a depletion of the ions on the anodic side of the Nafion membrane and an enrichment of the ions on the cathodic side. In other words, the ICP phenomenon is induced. Finally, in region C (the over-limiting region), the current increases approximately linearly with the voltage once again due to the destruction of the depletion zone as a result of electroconvection effects.[54] In general, the I-V curves shown in Fig. 3 confirm that the ICP phenomenon is induced in both μPADs. From inspection, ICP is induced at a voltage of approximately 57 V (or field strength 2.85×10^3 V/m) in the single-side printed μPAD and 40 V (or field strength 2×10^3 V/m) in the double-side printed device.

After determining the required voltage to trigger ICP, we performed the ICP experiment in which fluorescein (10^{-5} M) was concentrated in a two-side printed paper channel under the applied voltage of 200 V (or field strength 10^4 V/m). For conventional micro-nano channels, the ICP concentration mechanism has been applied to the anodic side[55] or cathodic side[24] of Nafion. For

the paper-based case, this ICP effect can also be observed from Fig. 4. It is seen that for the concentration on the anodic side of Nafion, the sample plug is in motion and dispersed in a short time. Papers consisting of cellulose fibers have complex structures, which renders friction between moving fluids and fibers. Therefore, samples in the mobile plug can often not be concentrated stably on the anodic side of Nafion. For this reason, we intend to concentrate sample concentration in a fixed position which is close to the cathodic side of the Nafion. For those targeted samples contain negatives ions, the Nafion is an ion-selective membrane which stops the negative ions to move through the perm-selective membrane to the left direction. At the same time, the negative ions are propelled to the left direction by the cathode side. Therefore the negatives ions will be accumulated near the right side of the Nafion. If the EOF has less speed to the right direction together with the electrophoretic effect, the contained negative ions sample will be focused more densely at the right side of the membrane. The lower EOF thereby minimizes the dispersion effect and enhances the concentration gain. Although adding PVP into the solution is one of methods for suppressing EOF,[42], however, we deliberately use shallow wax channel (compared to full-thickness paper channel) for (1) enhancing concentration effect; (2) making better signal visibility; (3) making more rapid heat dissipation,[42]; (4) suppressing EOF. To achieve these goals, we propose to use the shallow wax channel for suppressing EOF rather than the method adding PVP into the solution. Accordingly, this concentration technique is explored in the following detection step.

In developing the two-side printed μPAD, one of the objectives was to reduce the EOF speed. The two-side printed μPAD provides three waxed-surfaces to be contacted by fluids to yield lower zeta potentail,[41] thereby reducing the EOF speed. The validity of the proposed approach was evaluated by measuring the change in the current over time in both the one-side and two-side printed paper channels. In performing the measurement process, 10^{-2} M Tris buffer was dropped into the cathode reservoir and the paper channel using a pipette, and the time history of the current under an electric field of 10^4 V/m (or voltage 200 V) was measured after dropping 0.95×10^{-2} M

Tris buffer into the anode reservoir. For both devices, the current reduced over time as the lower-concentration Tris buffer in the anode reservoir gradually replaced the higher-concentration Tris buffer in the paper channel (Fig. 5). The current then remained at an approximately constant value once the channel was entirely full of low-concentration buffer. Dividing the total channel length (20 mm) by the time required for the low-concentration buffer to fill the entire channel, the EOF speed in the one- and two-side printed paper channels were determined to be 0.1003 ± 0.005018 mm/s (mobility $= (0.1003 \pm 0.005018) \times 10^{-7}$ (m^2 /V/s)) and 0.0480 ± 0.000941 mm/s (mobility $= (0.0480 \pm 0.000941) \times 10^{-7}$ (m^2/V/s)), respectively (as evaluated over eight runs). In other words, the results confirm that the two-side printed design gives rise to a lower EOF velocity because of a less zeta potential of the wax than that of the fiber.

Figure 6 shows the variation over time of the maximum fluorescence peak intensity and sample concentration in the single-side printed and two-side printed μPADs. Note that the concentration experiments were performed using a fluorescein sample with a concentration of 10^{-8} M in both cases. It is seen that for the two-side printed channel, the fluorescence peak intensity obtained on the cathodic side of the Nafion remains approximately constant for the first 14 min before rising rapidly to a maximum value after approximately 30 min. It is noted that the concentration gain achieved in the two-side printed channel (944-fold) is significantly higher than that achieved in the one-side printed channel (130-fold). Besides of a greater signal visibility in the shallower-channel design, the improved enrichment factor in such design can also be attributed not only to the lower EOF speed because of a less zeta potential of the wax than that the of fiber, but also to a greater confinement of the fixed amount of fluorescein within the channel due to its smaller geometry. Moreover, the lower current in the two-side printed paper channel results in a reduced Joule heating effect.[49] Consequently, the nanopore EOF is reduced, and hence the sample dispersion effect following the point of maximum intensity is also reduced.

The practical feasibility of the two-side printed μPAD was evaluated using an FITC-BSA

sample with an initial concentration of 10^{-8} M (see Fig. 7). As shown, the fluorescence peak intensity remained approximately constant for the first 8 min, and then increased to a maximum value after 28 min. The maximum concentration gain is around 835-fold. This enrichment factor is much higher than the results presented by Gong et al[35], Yang et al[36] and Phan et al[37], which are around 5-fold, 15-fold and 60-fold, respectively.

4. Conclusion

This paper has presented a two-side wax-printed μPAD for the enhanced ICP enrichment of low-concentration biomarkers. Compared to traditional wax-printed μPADs, in which the channel penetrates through the full thickness of the paper substrate, the two-sided wax-printing operation performed in the present study results in a paper channel which extends to a depth of just 50 μm. μPADs consist principally of cellulose fibers and thus have an extremely complex structure. As a result, a mobile sample plug can often not be concentrated stably on the anodic side of the permselective membrane due to a friction force between the fiber surface and the sample. Thus, in the present study, the sample is concentrated on the cathodic side of the Nafion. Notably, this approach has the benefit not only of producing a stable and stationary sample plug, but also avoids the need to balance tangential electric fields or to create a balance between electrophoresis and electroosmotic flow (or pressure-driven flow). The results have suggested that compared to a conventional μPAD with a full-thickness paper channel, the proposed shallow-channel design yields four important advantages for ICP-induced sample concentration, namely (1) a lower EOF velocity; (2) the ability to apply a higher driving voltage; (3) a greater confinement of the concentrated sample and (4) a greater signal visibility. In addition, it has been shown that while a conventional μPAD achieves a preconcentration factor of 130-fold for a pure fluorescein sample, the shallow-channel μPAD achieves a preconcentration factor of 944-fold. Moreover, for an FITC-BSA with an initial concentration of 10^{-8} M, a preconcentration factor of around 835-fold can be

obtained after approximately 28 min. The enrichment factor is much higher than most practical μPAD–based assays.[35-37] The stationary sample plug pre-concentration technique using two-side printed paper channel provides an attractive method for μPADs applications.

Acknowledgements

The authors gratefully acknowledge the financial support provided to this study by the Ministry of Science and Technology of Taiwan under Grant No. MOST 103-2221-E-006-093-MY3 and MOST 104-2221-E-006-154-MY3. In addition, the provision of microfabrication facilities by the National Nano-Device Laboratory, Tainan, Taiwan, is also much appreciated.

References

1. E. Carrilho, A. W. Martinez and G. M. Whitesides, *Anal. Chem.*, 2009, **81**, 7091-7095.
2. A. W. Martinez, S. T. Phillips, B. J. Wiley, M. Gupta and G. M. Whitesides, *Lab Chip*, 2008, **8**, 2146-2150.
3. A. W. Martinez, S. T. Phillips, M. J. Butte and G. M. Whitesides, *Angew. Chem. Int. Ed.*, 2007, **46**, 1318-1320.
4. A. W. Martinez, S. T. Phillips, E. Carrilho, S. W. Thomas III, H. Sindi and G. M. Whitesides, *Anal. Chem.*, 2008, **80**, 3699-3707.
5. X. Li, J. Tian, T. Nguyen and W. Shen, *Anal. Chem.*, 2008, **80**, 9131-9134.
6. D. A. Bruzewicz, M. Reches and G. M. Whitesides, *Anal. Chem.*, 2008, **80**, 3387-3392.
7. K. Abe, K. Suzuki and D. Citterio, *Anal. Chem.*, 2008, **80**, 6928-6934.
8. E. W. Fenton,M. R. Mascarenas, G. P. Lopez and S. S. Sibbett, *ACS Appl. Mater. Interfaces*, 2009, **1**, 124-129.

9. E. Fu, P. Kauffman, B. Lutz and P. Yager, *Sens. Actuators, B*, 2010, **149**, 325-328.

10. E. Carrilho, S. T. Phillips, S. J. Vella, A. W. Martinez and G. M. Whitesides, *Anal. Chem.,* 2009, **81**, 5990-5998.

11. M. M. Ali, S. D. Aguirre, Y. Xu, C. D. M. Filipe, R. Pelton and Y. Li, *Chem. Commun.,* 2009, 6640-6642.

12. P. B. Allen, S. A. Arshad, B. Li, X. Chen and A. D. Ellington, *Lab Chip*, 2012, **12**, 2951-2958.

13. U. H. Yildiz, P. Alagappan and B. Liedberg, *Anal. Chem.,* 2013, **85**, 820-824.

14. J. Yu, L. Ge, J. Huang, S. Wang and S. Ge, *Lab Chip*, 2011, **11**, 1286-1291.

15. J. Yu, S. Wang, L. Ge and S. Ge, *Biosens. Bioelectron.*, 2011, **26**, 3284-3289.

16. L. Ge, S. Wang, X. Song, S. Ge and J. Yu, *Lab Chip*, 2012, **12**, 3150-3158.

17. S. Wang, L. Ge, X. Song, J. Yu, S. Ge, J. Huang and F. Zeng, *Biosens. Bioelectron.*, 2012, **31**, 212-218.

18. J. Yan, L. Ge, X. Song, M. Yan, S. Ge and J. Yu, *Chem. Eur. J.*, 2012, **18**, 4938-4945.

19. M. Zhang, L. Ge, S. Ge, M. Yan, J. Yu, J. Huang and S. Liu, *Biosens. Bioelectron.,* 2013, **41**, 544-550.

20. Z. Nie, F. Deiss, X. Liu, O. Akbulut and G. M. Whitesides, *Lab Chip*, 2010, **10**, 3163-3169.

21. Z. Nie, C. A. Nijhuis, J. Gong, X. Chen, A. Kumachev, A. W. Martinez, M. Narovlyansky and G. M. Whitesides, *Lab Chip*, 2010, **10**, 477-483.

22. X. Chen, J. Chen, F. Wang, X. Xiang, M. Luo, X. Ji and Z. He, *Biosens. Bioelectron.*, 2012, **35**, 363-368.

23. M. Funes-Huacca, A. Wu, E. Szepesvari, P. Rajendran, N. Kwan-Wong, A. Razgulin, Y. Shen, J. Kagira, R. Campbell and R. Derda, *Lab Chip*, 2012, **12**, 4269-4278.

24. S. H. Ko, Y. A. Song, S. J. Kim, J. Han and K. H. Kang, *Lab Chip*, 2012, **12**, 4472-4482.

25. Y. C. Wang, A. L. Stevens and J. Han, *Anal. Chem.*, 2005, **77**, 4293-4299.

26. J. H. Lee, Y. A. Song and J. Han, *Lab Chip*, 2008, **8**, 596-601.

27. J. H. Lee, Y. A. Song, S. R. Tannenbaum and J. Han, *Anal. Chem.*, 2008, **80**, 3198-3204.

28. M. Pevarnik, M. Schiel, K. Yoshimatsu, I. V. Vlassiouk, J. S. Kwon, K. J. Shea and Z. S. Siwy, *ACS Nano*, 2013, **7**, 3720-3728.

29. G. I. Abelev and E. R. Karamova, *Mol. Immunol.*, 1989, **26**, 41-47.

30. B. Y. Moghadam, K. T. Connelly and J. D. Posner, *Anal. Chem.*, 2014, **86**, 5829-5837.

31. D. S. Burgi and R. L. Chien, *Anal. Chem.*, 1991, **63**, 2042-2047.

32. J. P. Quirino and S. Terabe, *Science*, 1998, **282**, 465-468.

33. I. Rubinstein and L. Shtilman, *J. Chem. Soc., Faraday Trans. 2*, 1979, **75**, 231-246.

34. Z. Slouka, S. Senapati and H. C. Chang, *Annu. Rev. Anal. Chem.*, 2014, **7**, 317-335.

35. M. M. Gong, P. Zhang, B. D. MacDonald and D. Sinton, *Anal. Chem.*, 2014, **86**, 8090-8097.

36. R. J. Yang, H. H. Pu and H. L. Wang, *Biomicrofluidics*, 2015, **9**, 014122.

37. D. T. Phan, S. A. M. Shaegh, C. Yang and N. T. Nguyen, *Sens. Actuators B Chem.*, 2016, **222**, 735-740.

38. M. M. Gong, R. Nosrati, M. C. S. Gabriel, A. Zini and D. Sinton, *J. Am. Chem. Soc.*, 2015, **137**, 13913-13919.

39. Y. Lu, W. Shi, L. Jiang, J. Qin and B. Lin, *Electrophoresis*, 2009, **30**, 1497-1500.

40. A. W. Martinez, S. T. Phillips and G. M. Whitesides, *Anal. Chem.*, 2010, **82**, 3-10.

41. J. M. Molho, A. E. Herr, M. Desphande, J. R. Gilbert, M. G. Garguilo, P. H. Paul, P. M. John, T. M. Woudenberg and C. Connel, *Proc. ASME (MEMS)*, 1998, **66**, 69-76.

42. T. Rosenfeld and M. Bercovici, *Lab Chip*, 2014, **14**, 4465-4474.

43. Merck Millipore, *Rapid Lateral Flow Test Strips Considerations for Product Development*, EMD Millipore Corporation, Billerica, MA., Germany, 2013.

44. S. Zeng, C. H. Chen, J. C. M. Jr. and J. G. Santiago, *Sens. Actuators B*, 2001, **79**, 107-114.

45. R. Pelton, *TrAC*, 2009, **28**, 925-942.

46. A. K. Yetisen, M. S. Akram and C. R. Lowe, *Lab Chip*, 2013, **13**, 2210-2251.

47. E. Fu, S. A. Ramsey, P. Kauffman, B. Lutz and P. Yager, *Microfluid. Nanofluid.*, 2011, **10**, 29-35.

48. X. Huang, M. J. Gordon and R. N. Zare, *Anal. Chem.*, 1988, **60**, 1837-1838.

49. D. Wu and A. J. Steckl, *Lab Chip*, 2009, **9**, 1890-1896.

50. V. Liu, Y. A. Song and J. Han, *Lab Chip*, 2010, **10**, 1485-1490.

51. J. H. Lee, Y. A. Song and J. Han, *Lab Chip*, 2008, **8**, 596-601.

52. S. J. Kim and J. Han, *Anal. Chem.*, 2008, **80**, 3507-3511.

53. A. Mani, T. A. Zangle and J. G. Santiago, *Langmuir*, 2009, **25**, 3898-3908.

54. I. Rubinstein, E. Staude and O. Kedem, *Desalination*, 1988, **69**, 101-104.

55. R. S. Foote, J. Khandurina, S. C. Jacobson and J. M. Ramsey, *Anal. Chem.*, 2005, **77**, 57-63.

List of Figures

Figure 1. Schematic illustrations of fabrication procedure for: (a) one-side printed μPAD and (b) two-side printed μPAD. (c) Dimensions of one- and two-side printed μPADs. (d) Microscope image of channel cross-section in two-side printed μPAD.

Figure 2. Photographs of ICP-based μPAD.

Figure 3. Current-voltage curves for one- and two-side printed μPADs. (Note that measurements were obtained using fluorescein solution (10^{-8} M) and tris buffer (10^{-2} M). Moreover, the voltage was increased from 0 to 210 V (field strength from 0 to 1.05×10^4 V/m) in 105 discrete steps over a period of 600 s.)

Figure 4. Mobility difference between the fluorescein concentration on the anodic and cathodic side of Nafion in two-side printed μPAD under applied voltage of 200V (electric field 10^4 V/m). Note that original fluorescein concentration is 10^{-5} M and all observations with corresponding time were made using the same set of ICP experiment. The concentrated sample plug is in motion and dispersed in short time in the anodic side, on the other hand, the cathodic side shows a stationary concentrated sample plug.

Figure 5. Measurement of EOF speed in one- and two-side wax-printed μPADs. Each current value is averaged over N=8 measurements, and the error bars represent one standard deviation.

Figure 6. Variation of maximum fluorescence peak intensity and corresponding sample concentration over time in one- and two-side printed μPADs under applied voltage of 200V

(electric field 10^4 V/m). Note that original (diluted) fluorescein concentration is 10^{-8} M and the top-left inset shows calibration curves for fluorescein in both one- and two-side printed μPADs. Each intensity value is averaged over N=4 measurements, and the error bars represent one standard deviation. Refer to the animation video 1 and 2.

Figure 7. Variation of maximum FITC-BSA peak intensity and corresponding sample concentration over time in two-side printed μPAD under applied voltage of 200V (electric field 10^4 V/m). Note that original (diluted) FITC-BSA concentration is 10^{-8} M and the top-left inset shows calibration curve for FITC-BSA in two-side printed μPAD. Each intensity value is averaged over N=4 measurements, and the error bars represent one standard deviation.

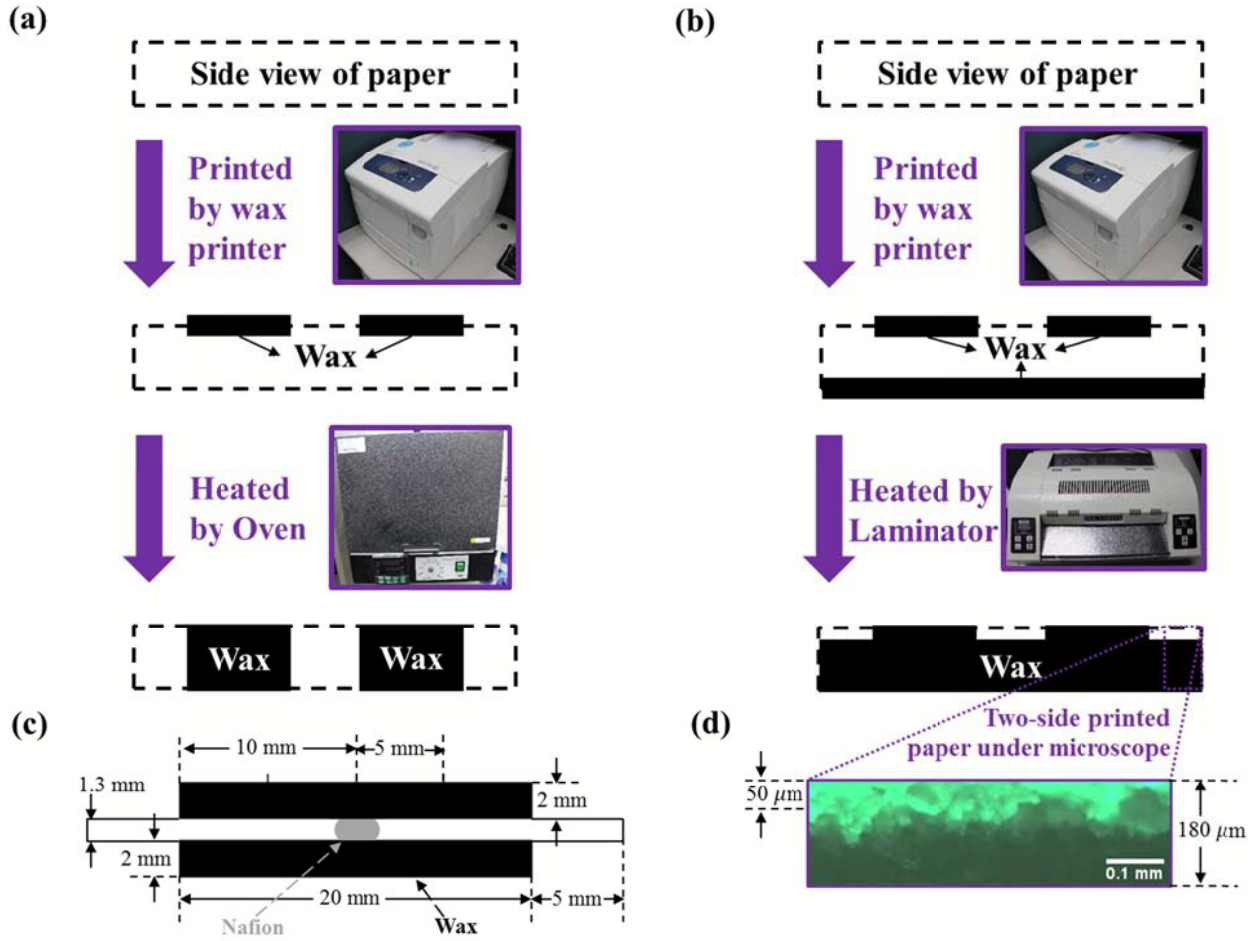

Figure 1. Schematic illustrations of fabrication procedure for: (a) one-side printed μPAD and (b) two-side printed μPAD. (c) Dimensions of one- and two-side printed μPADs. (d) Microscope image of channel cross-section in two-side printed μPAD.

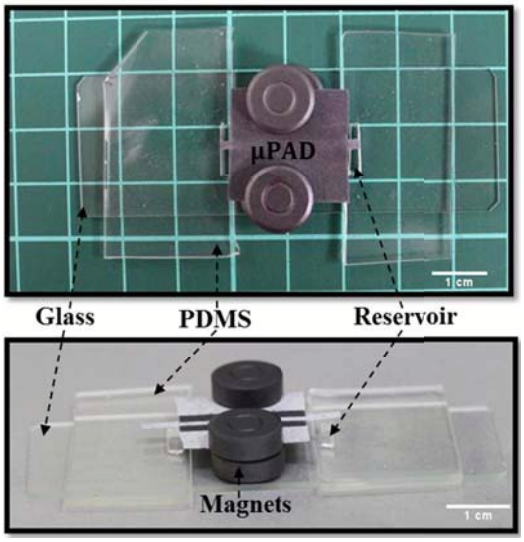

Figure 2. Photographs of ICP-based μPAD.

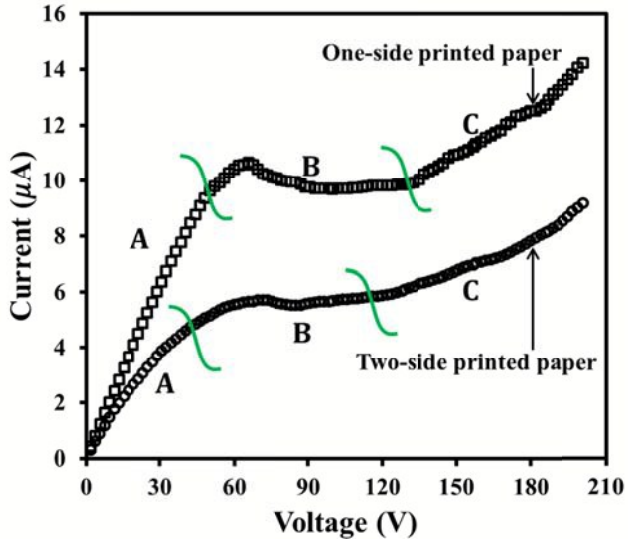

Figure 3. Current-voltage curves for one- and two-side printed μPADs. Note that measurements were obtained using fluorescein solution (10^{-8} M) and tris buffer (10^{-2} M). Moreover, the voltage was increased from 0 to 210 V (field strength from 0 to 1.05×10^{4} V/m) in 105 discrete steps over a period of 600 s.

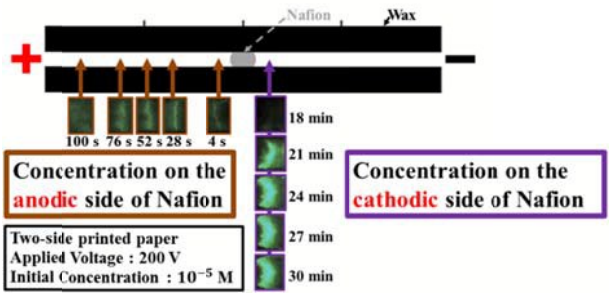

Figure 4. Mobility difference between the fluorescein concentration on the anodic and cathodic side of Nafion in two-side printed μPAD under applied voltage of 200V (electric field 10^4 V/m). Note that original fluorescein concentration is 10^{-5} M and all observations with corresponding time were made using the same set of ICP experiment. The concentrated sample plug is in motion and dispersed in short time in the anodic side, on the other hand, the cathodic side shows a stationary concentrated sample plug.

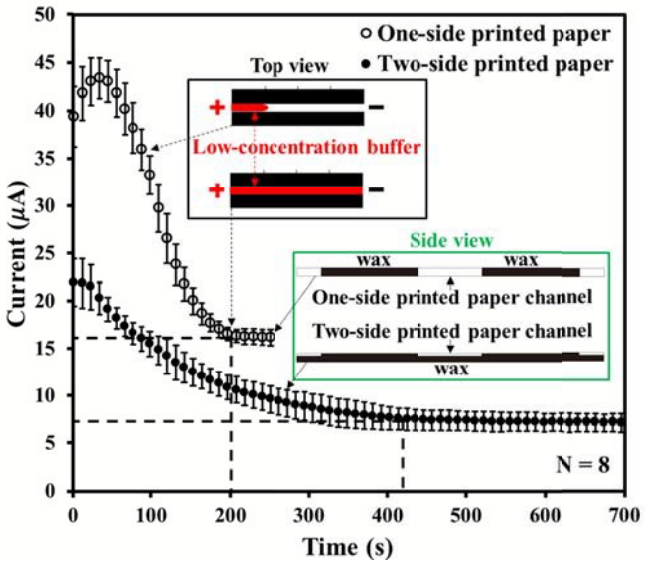

Figure 5. Measurement of EOF speed in one- and two-side wax-printed μPADs. Each current value is averaged over N=8 measurements, and the error bars represent one standard deviation.

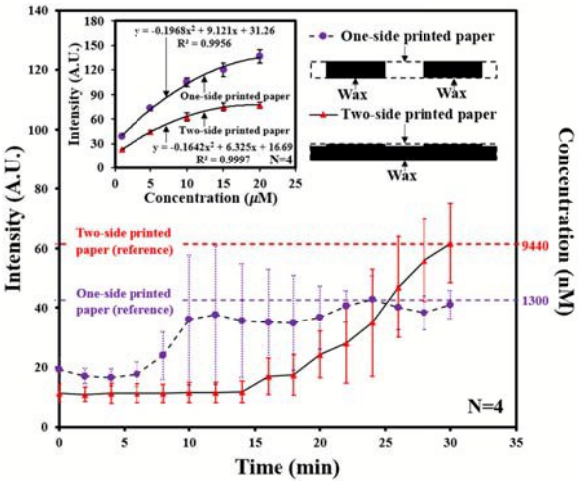

Figure 6. Variation of maximum fluorescence peak intensity and corresponding sample concentration over time in one- and two-side printed μPADs under applied voltage of 200V (electric field 10^4 V/m). Note that original (diluted) fluorescein concentration is 10^{-8} M and the top-left inset shows calibration curves for fluorescein in both one- and two-side printed μPADs. Each intensity value is averaged over N=4 measurements, and the error bars represent one standard deviation. Refer to the animation video 1 and 2.

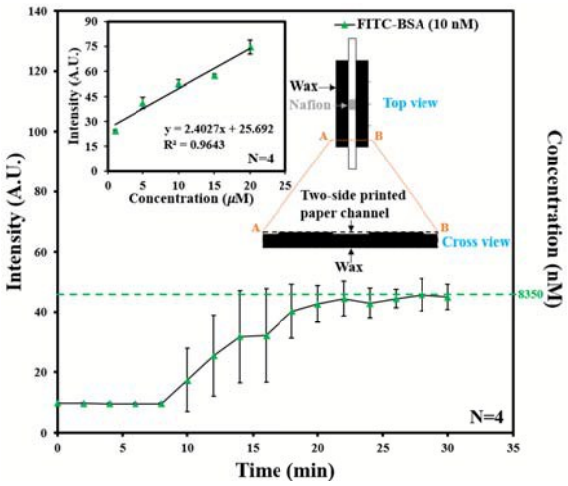

Figure 7. Variation of maximum FITC-BSA peak intensity and corresponding sample concentration over time in two-side printed μPAD under applied voltage of 200V (electric field 10^4 V/m). Note that original (diluted) FITC-BSA concentration is 10^{-8} M and the top-left inset shows calibration curve for FITC-BSA in two-side printed μPAD. Each intensity value is averaged over N=4 measurements, and the error bars represent one standard deviation.